J|A|C|S COMMUNICATIONS

Published on Web 11/12/2010

Polyhedral 50-Facet Cu_2O Microcrystals Partially Enclosed by {311} High-Index Planes: Synthesis and Enhanced Catalytic CO Oxidation Activity

Mei Leng,[†,‡] Mingzhu Liu,[†,‡] Yibo Zhang,[†,‡] Zhenqing Wang,[†,‡] Chao Yu,[†,‡] Xiangguang Yang,[†] Hongjie Zhang,[*,†] and Cheng Wang[*,†]

State Key Laboratory of Rare Earth Resource Utilization, Changchun Institute of Applied Chemistry, Chinese Academy of Sciences, 5625 Renmin Street, Changchun, Jilin 130022, P. R. China, and Graduate School of the Chinese Academy of Sciences, Beijing 100039, P. R. China

Received July 29, 2010; E-mail: cwang@ciac.jl.cn; hongjie@ciac.jl.cn

Abstract: Micro- and nanoparticles with high-index facets may exhibit higher chemical activities that are of great importance in practical applications. Cuprite is a potential alternative to expensive noble metals as the catalyst for CO oxidation at moderate temperatures. We report here a solution based approach to the preparation of unusual polyhedral 50-facet Cu_2O microcrystals with a morphological yield higher than 70%. It has been revealed that the concentration of OH^- and the volume ratio of polar organic solvent to water in the mixed solvent play crucial roles in controlling the morphology of Cu_2O microcrystals. The formation of the 50 facets could be geometrically viewed as the truncation of all the 24 vertices of a small rhombicuboctahedron having 26 facets. When growing from solutions, however, the anisotropic growth rates along the ⟨100⟩, ⟨110⟩, and ⟨111⟩ directions might be responsible for the formation of this morphology. The Miller index of the 24 nearly isosceles trapezoids could be assigned to {311} planes based on geometrical analysis and was verified by simulated models using the WinXmorph software and supported by TEM and ED observations. Compared with other polyhedral Cu_2O microcrystals, the as-prepared microcrystals showed a higher specific catalytic rate toward CO oxidation.

Micro- and nanoscale materials with well-defined shapes are usually bound by planes with low surface energies, as high energy surfaces have larger crystal-growth rates along their normal directions and tend to disappear from final appearances.[1,2] For materials with a cubic structure such as noble metals,[3,4] lead chalcogenides,[5,6] and flurites,[7] many micro- and nanostructures with exotic shapes including five Platonic polyhedra, some Archimedean solids, rhombic dodecahedron, twinned or truncated polyhedra, and two-dimensional prisms as well as plates have been successfully prepared through a variety of synthetic methods. Their surfaces are usually enclosed by low-index {100}, {110}, or {111} planes. Recently, tetrahexahedral Pt nanocrystals with 24 high-index facets exhibiting higher catalytic activities toward the electro-oxidations of formic acid and ethanol were synthesized using an electrochemical process.[8] Inspired by this work, gold nanoparticles with 24 high-index facets (both tetrahexahedral and trisoctahedral)[9−11] and octahedral tin dioxide nanocrystals with high-index facets of {221}[12] have been achieved by different groups using solution reduction processes. The high Miller indices of crystal facets contain atomic height steps, which separate the terraces of atoms and are abundant with ledges or kinks. Such structural characteristics endow them with high chemical activity and may show advantages in heterogeneous catalytic reactions.[13] In this work, we report a solution reduction process to the synthesis of Cu_2O microcrystals with 50 facets that show an enhanced specific catalytic rate toward CO oxidation due to the presence of 24 high-index {311} facets among their 50 facets.

Cuprous oxide (Cu_2O), also known as cuprite, has a cubic crystal structure in which oxygen atoms form a body-centered cubic lattice while copper atoms form a face-centered cubic lattice. Being one of the earliest semiconducting materials, it is a p-type semiconductor having a direct band gap of 2.17 eV and could find practical applications in solar energy conversion,[14] hydrogen production by photocatalysis of water,[15,16] and lithium-ion batteries as electrode material.[17] The use of Cu_2O in antifouling coatings for marine ship hulls has experienced a resurgence since the ban of tributyltin in 2003 because it is relatively benign to both human and environment.[18] It is also a promising alternative to expensive noble metals as the catalyst for CO oxidation at moderate temperatures, owing to its higher natural abundance and lower price. CO oxidation is of practical importance in many industrial processes such as water-gas shifting,[19,20] automotive exhaust control,[21] and toxic gas removal in polymeric electrolyte membrane fuel cell.[22−24] Due to the propensity of Cu_2O toward valence variations, it tends to seize or release surface lattice oxygen when oxidized or reduced accordingly. Therefore it is expected to exhibit higher CO oxidation activities than CuO and Cu.[25] Similar to noble metals, many shapes of micro- and nanoscale particles of Cu_2O enclosed by low-index facets have been accomplished by either electro- or solution-based chemical approaches.[26−35]

The synthesis of target polyhedral Cu_2O microcrystals was fulfilled in an alkaline solution using D-(+)-glucose as a reducing agent. The deployed temperature was 60 °C, and the reaction time was in the range of 10−15 min. Details of the experiments are provided in the Supporting Information. The resultant product is a pure cubic phase of Cu_2O as confirmed by its X-ray diffraction pattern (XRD) (Figure S1). Under field emission scanning electron microscopy (FESEM) investigations, Cu_2O microparticles having polyhedral morphology could be observed (Figure 1A). Closer observations of each individual polyhedra with different polygons facing up revealed the edge-sharing connection relationships among the four kinds of polygons on their surfaces (Figure 1B−1E). Each square is connected with four trapezoids, and each trapezoid is connected with one square and three hexagons. There are two kinds of hexagons. One is connected with three hexagons and three trapezoids and termed as $H_{3,3}$, while the other one is connected with two hexagons and four trapezoids and termed as $H_{2,4}$. The polyhedron is covered by 6 squares, 8 $H_{3,3}$ hexagons, 12 $H_{2,4}$ hexagons, and 24 trapezoids, and therefore the total number of

[†] State Key Laboratory of Rare Earth Resource Utilization, Chinese Academy of Sciences.
[‡] Graduate School of the Chinese Academy of Sciences.

10.1021/ja106788x

polygons is 50. In addition, the derived numbers of edges and vertices are 144 and 96 respectively. The relation of the numbers of faces (F), edges (E), and vertices (V) follows Euler's rule ($V + F - E = 2$) for a typical convex polyhedron.

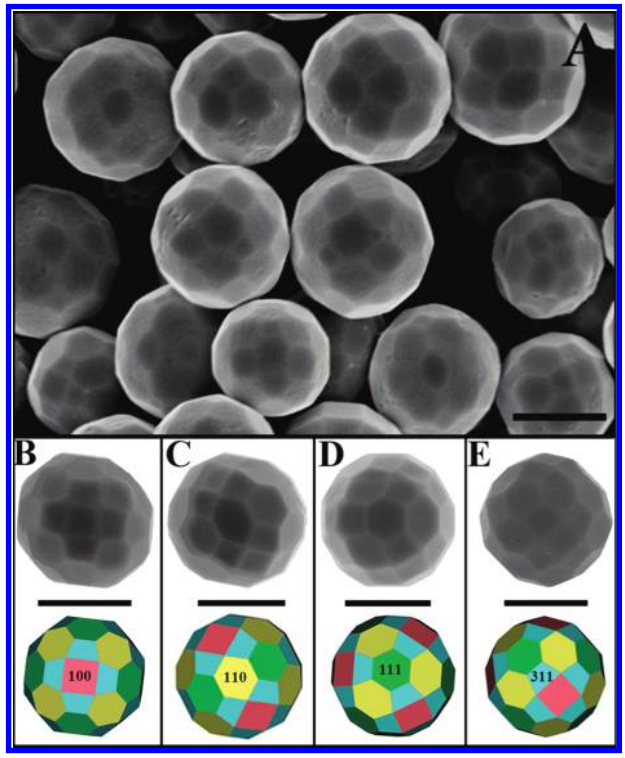

Figure 1. Typical FESEM images of as-synthesized polyhedral 50-facet Cu_2O microcrystals (A) and observed and simulated (bottom) individual polyhedra with different polygons facing up (B−E). Scale bar = 2.0 μm.

Geometrically, the 50-facet polyhedron is inherently correlated with a small (not great) rhombicuboctahedron (hereafter abbreviated as sR), an Archimedean polyhedron with 24 vertices, 26 facets, and 48 edges, as the truncation of all 24 vertices of a sR would result in a 50-facet polyhedron (Scheme S1A). The eight nearly regular $H_{3,3}$ hexagons (Figure 1D) could be formed by truncating 1/3 of the sides of the (111) equilateral triangle planes around each vertex of sR. The squares could be viewed as cutting four isosceles right triangles from the {100} squares of sR with half the area left. Since each (110) square plane on sR shares two sides with two {100} square planes and the other two sides with two {111} triangle planes, the $H_{2,4}$ hexagon would be formed by connecting the cutting points of its adjacent sides. Such inequilateral truncations around each vertex lead to the formation of an isosceles trapezoid on the surface of sR. The calculated dihedral angel between a (100) square plane and one trapezoid is 24.38° (Scheme S1B), which is close to the ideal angle (25.24°) between the (100) and (311) planes for cubic structures. Therefore, according to Steno's law, the trapezoids might be tentatively assigned to {311} facets. Using the WinXmorph software developed by Werner Kaminsky,[36] simulated 50-facet polyhedra with different polygons facing up could be drawn by setting the distances at 1.0 for all three low-index planes and 1.03 for {311} planes. All four simulated models (bottom of Figure 1) match well with corresponding observed individual particles. It should be pointed out that different truncations may occur and lead to the formation of other facets with high-index planes; similar observations were reported earlier.[8−12] Precise assignments of different truncated planes require more calculations or direct observations under high resolution transmission electron microscopy (HRTEM).[37] A panorama view of the product shows that the polyhedral microparticles with 50 facets coexisted with some smaller sR particles as well as other poorly developed polyhedral particles. The calculated percentages of the 50-facet, sR, and poorly developed particles are 73, 15, and 12% respectively by counting 173 particles (Figure S2).

The products were further characterized by TEM. The particles showed nearly circular contours if randomly oriented (results not shown), as expected from their appearance in Figure 1. By tilting the orientations of three particles, an octagon projecting from the [100] direction and two different dodecagons projecting from both [110] and [111] directions can be observed (Figure 2). The orientations of the particles were confirmed by their corresponding electron diffractions (Figure 2), which also suggest that the obtained Cu_2O particles are single crystals. The interior angles of the octagon and the dodecagon projecting from the [110] direction could be assigned to some dihedral angles of adjacent facets. Since the measured dihedral angles are close to the theoretical dihedral values between corresponding facets, these two polygons have similar contours to the two models projected from the same directions. Although not all of the interior angles of the dodecagon projecting from [111] can be assigned to the dihedral angles between facets on the microcrystal surface, it still resembles the model projecting from the same direction in terms of geometry (Figure S3A−S3C). Due to their large particle sizes, no HRTEM image could be directly obtained. After smashing the particles, lattice fringes of (200), (110), and (111) can be seen (Figure S3D). But the lattice fringe of (311) (d = 1.29 Å) was still not observable because it is beyond the resolution limit (1.9 Å) of our TEM instrument.

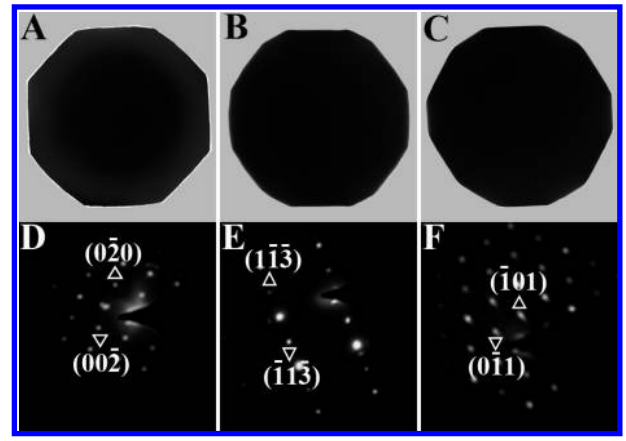

Figure 2. TEM images and corresponding electron diffraction patterns of three polyhedral 50-facet microcrystals projecting from [100] (A and D), [110] (B and E), and [111] (C and F) directions.

Most likely the synthesis of polyhedral 50-facet Cu_2O microparticles follows a kinetic-controlled mechanism. We started with a low concentration of copper salt, e.g., 6.0 mmol/L, and used a weak reducing agent. These choices allowed a low supersaturation degree during the reducing process and made a kinetic-controlled synthesis feasible. Among all the other parameters, the concentration of OH^- and the volume ratio of ethanol (or other polar organic solvents) to water (R_{ew}) in the mixed solvent were found to play key roles in determining the morphology and particle size of Cu_2O. In this study, the ethanol−water system has been studied comprehensively. The optimized conditions were given in the typical synthetic process in the Supporting Information. Briefly, the suitable concentration of OH^- was in the range of 0.8 to 1.0 mol/L while the R_{ew} was around 1:24. The addition of a small volume of polar organic solvent has been proven to be indispensable for our

synthesis. Mixed alcohols and dimethyl formamide have been also tested for the synthesis of target Cu_2O microcrystals (Figure S4), and viscosity measurements showed that the viscosities of all similar solutions decrease significantly (Figure S5), compared with that of a pure NaOH aqueous solution. The decreased viscosities may enhance the diffusions of the reactants (or growth units) and benefit the formation of the unique polyhedral morphology in these reaction systems. Further decreasing the viscosities via increasing the amount of ethanol in the reaction systems would lead to the formation of other morphologies as shown in Figure S6. However, both the particle size and morphology of the 50-facet Cu_2O microcrystals were found to be independent of the anions of investigated copper salts ($CuCl_2$, $CuSO_4$, $Cu(NO_3)_2$, and $Cu(CH_3COO)_2$) or cations of the bases (KOH or NaOH). Certainly, the reactions are affected by the reaction temperature and time. As the reaction temperature deviated from 60 °C, the shapes of the resultant products using the same recipe for the typical synthetic process became less uniform due to the break of the established kinetic conditions. When the reaction time was less than 2 min, XRD results showed that the reaction could not be completed for peaks of CuO still remained (Figure S7). A longer reaction time would cause the deterioration of the morphology or redissolution of the products into the solution by dissolved oxygen in the reaction solution from air.

The involved chemical reactions are fairly simple. Initially, when OH^- was added into the mixed solvent containing copper salt, $Cu(OH)_2$ was first precipitated from the solution and then decomposed into black CuO at 60 °C. Upon the introduction of D-(+)-glucose, CuO was reduced into Cu_2O likely via the soluble $Cu(OH)_4^{2-}$ species. To address the formation mechanism of the 50-facet polyhedron, the shape evolution of Cu_2O microcrystals was examined by tuning both the concentration of OH^- and R_{ew}. When R_{ew} was set as 1:24, increasing the concentration of OH^- in the reaction system from 0.05 to 1.0 mol/L would alter the morphology of Cu_2O from a cube to an sR and eventually to the titled 50-facet polyhedron (Figure S8). On the other hand, when the concentration of OH^- was set as 1.0 mol/L, varying R_{ew} from 0 to 1.17 caused a progressive morphological change from the sR to 50-facet polyhedron, tetradecahedron, and octahedrons (Figure S6). The solubility of cuprite in aqueous media depends on the pH value and temperature of the media.[38] Under alkaline conditions, increasing the concentration of OH^- would yield more soluble copper ions in the solutions, which may provide an appropriate growth rate for forming the polyhedral Cu_2O microcrystals. In addition, the electrostatic interactions between OH^- and the surface copper(I) atoms on the three low-index planes of Cu_2O might level off the surface energy difference among the three low-index planes. In the above geometrical analysis, we mentioned that the formation of the 50-facet polyhedron could be viewed as a result of truncating 24 vertices of an sR. A different approach might occur for the growth of polyhedral 50-facet Cu_2O microcrystals in the synthetic route. Further growths of {100}, {110}, and {111} planes on small sR Cu_2O microcrystals might be responsible for the formation of the titled polyhedral microcrystals. Experimentally, we did observe the coexistence of sR, slightly truncated sR Cu_2O microcrystals, and 50-facet polyhedral Cu_2O microcrystals with a gradual increase of particle size in a single batch (Figure S9). Different truncation degrees on the three low-index planes further suggest that the growth rates along the perpendicular directions of these three planes follow a sequence of {100} > {110} ≈ {111}. In addition, during the synthetic process, the {311} planes might have a lower surface energy because the surface unsaturated copper(I) cations might be coordinated by OH^- anions in the alkaline solution.

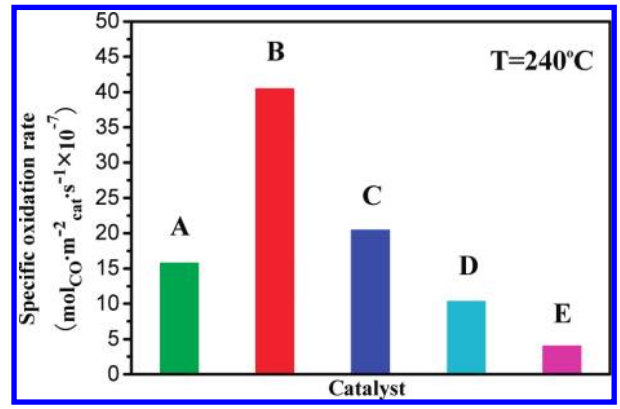

Figure 3. Specific oxidation rates of CO over Cu_2O microcrystals (A) sR, (B) polyhedral 50-facet, (C) rhombic dodecahedral, (D) octahedral, and (E) cubic in a 4 vol % CO/3 vol % O_2/93 vol % Ar stream at 240 °C.

The catalytic CO oxidation over the as-obtained 50-facet polyhedral Cu_2O microcrystals was evaluated in a CO/O_2/Ar stream (Figure S10). For comparison, same amounts of cubic, octahedral, rhombic dodecahedral, and sR Cu_2O microcrystals were also tested (Figures S10 and S11). The rhombic dodecahedral microcrystals, which could not be obtained in our system, were prepared using a reported protocol.[30] In order to eliminate the size effect, the specific catalytic CO oxidation rates over different microparticles were calibrated with surface areas using their average particle sizes (Figure 3). These results clearly revealed that the CO oxidation over Cu_2O microcrystals exhibits a morphological dependence on catalytic activity. The highest specific catalytic rate over a polyhedral 50-facet Cu_2O microcrystal might be attributed to the presence of high-index {311} planes on their surfaces. Assuming the product to contain only polyhedral 50-facet Cu_2O microcrystals, the specific catalytic CO oxidation rate on the {311} facet was estimated to be 8.8×10^{-6} $mol·m^{-2}_{cat}·s^{-1}$ (see the calculation following Figure S10), which is significantly higher than those over rhombic dodecahedral, octahedral, and cubic microcrystals with corresponding {110}, {111}, and {100} facets (Figure 3). Using the commonly so-called "microfaceted" method,[13] this high-index plane could be described by a terrace × step notion as 2(100) × (111) and would have two units of (100) on the terrace and one unit of (111) at the step[39] (the surface structures of these four different facets were shown in Figure S12). The calculated surface Gibbs free energy of this plane, on the basis of the "ab initio atomisitic thermodynamic",[39] was larger than those of the most stable terminations for the various low-index surfaces, i.e., Cu_2O(100):O, Cu_2O(110):CuO, and Cu_2O(111)−Cu_{cus} (coordination of unsaturated copper) under an oxygen-rich atmosphere. Yet, caution should be exercised in interpreting the varied catalytic activities among particles covered with different planes because no direct measurement could be attained for determining the exact termination of each plane on polycrystalline microparticles. XRD patterns of 50-facet Cu_2O microcrystals, before and after CO oxidation (Figure S1), are similar. XPS spectra indicated that the surface of Cu_2O was covered by a relatively more stable CuO phase. The thickness of this layer is assumed to be less than 5 nm as only the binding energy of Cu $2p_{3/2}$ (932.4 eV) appeared on the XPS spectrum after removing ~5 nm from the surface of the product via an ion bombarding treatment (Figure S13). A similar phenomenon has been found in one-dimensional Cu_2O nanostructures.[40] The formation of the thin CuO layer is due to the exposure of Cu_2O to the air during the washing and drying process. During the CO catalytic oxidation process in the CO/O_2/Ar atmosphere, CuO could be easily

reduced back to Cu_2O and the interference of CuO on catalytic activity might be negligible.

In conclusion, polyhedral Cu_2O microcrystals with 50 facets have been prepared in alkaline solutions under mild experimental conditions. The concentration of OH^- and the volume ratios of polar organic solvents to water in the mixed solvent played key roles in determining the morphology and particle size of Cu_2O. For the latter case, a small amount of coexisting organic solvents could decrease the viscosities of the reaction media significantly with which the diffusions of the reactants were increased and an appropriate kinetic controlled growth condition could be attained. Geometrical analysis, TEM and ED results, and simulations from the WinXmorph software suggested that the surface of the microcrystals was enclosed by high-index {311} facets in addition to low-index {100}, {110}, and {111} facets. The observed enhanced specific catalytic rate toward CO oxidation over the polyhedral 50-facet Cu_2O microcrystals was ascribed to the presence of these high-index facets.

Acknowledgment. This work is supported by the National Basic Research Program of China (2007CB925101) and the NSFC Fund for Creative Research Group (20921002).

Supporting Information Available: Detailed experimental procedures; results of XRD, FESEM, TEM, HRTEM, scheme, viscosity, XPS, and catalytic CO oxidation. This material is available free of charge via the Internet at http://pubs.acs.org.

References

(1) Lee, K.; Kim, M.; Kim, H. *J. Mater. Chem.* **2010**, *20*, 3791–3798.
(2) Xiong, Y.; Wiley, B. J.; Xia, Y. *Angew. Chem., Int. Ed.* **2007**, *46*, 7157–7159.
(3) Xia, Y.; Xiong, Y.; Lim, B.; Skrabalak, S. E. *Angew. Chem., Int. Ed.* **2009**, *48*, 60–103.
(4) Tao, A. R.; Habas, S.; Yang, P. *Small* **2008**, *4*, 310–325.
(5) Mokari, T.; Zhang, M.; Yang, P. *J. Am. Chem. Soc.* **2007**, *129*, 9864–9865.
(6) Lee, S.-M.; Jun, Y.-W.; Cho, S.-N.; Cheon, J. *J. Am. Chem. Soc.* **2002**, *124*, 11244–11245.
(7) Sun, X.; Li, Y. *Chem. Commun.* **2003**, 1768–1769.
(8) Tian, N.; Zhou, Z.; Sun, S.; Ding, Y.; Wang, Z. *Science* **2007**, *316*, 732–735.
(9) Ma, Y.; Kuang, Q.; Jiang, Z.; Xie, Z.; Huang, R.; Zheng, L. *Angew. Chem., Int. Ed.* **2008**, *47*, 8901–8904.
(10) Ming, T.; Feng, W.; Tang, Q.; Wang, F.; Sun, L.; Wang, J.; Yan, C. *J. Am. Chem. Soc.* **2009**, *131*, 16350–16351.
(11) Kim, D. Y.; Im, S. H.; Park, O. O. *Cryst. Growth Des.* **2010**, *10*, 3321–3323.
(12) Han, X.; Jin, M.; Xie, S.; Kuang, Q.; Jiang, Z.; Jiang, Y.; Xie, Z.; Zheng, L. *Angew. Chem., Int. Ed.* **2009**, *48*, 9180–9183.
(13) Van Hove, M. A.; Somorjai, G. A. *Surf. Sci.* **1980**, *92*, 489–518.
(14) Musa, A. O.; Akomolafe, T.; Carter, M. J. *Sol. Energy Mater. Sol. Cells* **1998**, *51*, 305–316.
(15) Hara, M.; Kondo, T.; Komoda, M.; Ikeda, S.; Shinohara, K.; Tanaka, A.; Kondo, J. N.; Domen, K. *Chem. Commun.* **1998**, 357–362.
(16) Nian, J.-N.; Hu, C.-C.; Teng, H. *Int. J. Hydrogen Energy* **2008**, *33*, 2897–2903.
(17) Poizot, P.; Laruelle, S.; Grugeon, S.; Dupont, L.; Tarascon, J. M. *Nature* **2000**, *407*, 496–499.
(18) Chambers, L. D.; Stokes, K. R.; Walsh, F. C.; Wood, R. J. K. *Surf. Coat. Technol.* **2006**, *201*, 3642–3652.
(19) Campbell, C. T.; Daube, K. A. *J. Catal.* **1987**, *104*, 109–119.
(20) Colbourn, E.; Hadden, R. A.; Vandervell, H. D.; Waugh, K. C.; Webb, G. *J. Catal.* **1991**, *130*, 514–527.
(21) Oudenhuijzen, M. K.; Kooyman, P. J.; Tappel, B.; van Bokhoven, J. A.; Koningsberger, D. C. *J. Catal.* **2002**, *205*, 135–146.
(22) Xie, X.; Li, Y.; Liu, Z.-Q.; Haruta, M.; Shen, W. *Nature* **2009**, *458*, 746–749.
(23) Hickman, D. A.; Schmidt, L. D. *Science* **1993**, *259*, 343–346.
(24) Xiao, T.-C.; Hanif, A.; York, A. P. E.; Nishizaka, Y.; Green, M. L. H. *Phys. Chem. Chem. Phys.* **2002**, *4*, 4549–4554.
(25) Huang, T.-J.; Tsai, D.-H. *Catal. Lett.* **2003**, *87*, 173–178.
(26) Sui, Y.; Fu, W.; Zeng, Y.; Yang, H.; Zhang, Y.; Chen, H.; Li, Y.; Li, M.; Zou, G. *Angew. Chem., Int. Ed.* **2010**, *49*, 4282–4285.
(27) Zhang, D.-F.; Zhang, H.; Guo, L.; Zheng, K.; Han, X.-D.; Zhang, Z. *J. Mater. Chem.* **2009**, *19*, 5220–5225.
(28) Pang, H.; Gao, F.; Lu, Q. *Chem. Commun.* **2009**, 1076–1078.
(29) Zhao, X.; Bao, Z.; Sun, C.; Xue, D. *J. Cryst. Growth* **2009**, *311*, 711–715.
(30) Liang, X.; Gao, L.; Yang, S.; Sun, J. *Adv. Mater.* **2009**, *21*, 2068–2071.
(31) Zhou, W.; Yan, B.; Cheng, C.; Cong, C.; Hu, H.; Fan, H.; Yu, T. *CrystEngComm* **2009**, *11*, 2291–2296.
(32) Kuo, C.-H.; Huang, M. H. *J. Am. Chem. Soc.* **2008**, *130*, 12815–12820.
(33) Tan, Y.; Xue, X.; Peng, Q.; Zhao, H.; Wang, T.; Li, Y. *Nano Lett.* **2007**, *7*, 3723–3728.
(34) Siegfried, M. J.; Choi, K.-S. *J. Am. Chem. Soc.* **2006**, *128*, 10356–10357.
(35) Matthew, J. S.; Kyoung-Shin, C. *Angew. Chem., Int. Ed.* **2005**, *44*, 3218–3223.
(36) Kaminsky, W. *J. Appl. Crystallogr.* **2005**, *38*, 566–567. http://cad4.cpac.washington.edu/WinXMorphHome/WinXMorph.htm.
(37) Zhou, Z.-Y.; Tian, N.; Huang, Z.-Z.; Chen, D.-J.; Sun, S.-G. *Faraday Discuss.* **2009**, *140*, 81–92.
(38) Palmer, D. A.; Bénézeth, P. Solubility of copper oxides in water and steam, *14th International Conference on the Properties of Water and Steam in Kyoto*, 2004, 491−496.
(39) Soon, A.; Cui, X.-Y.; Delley, B.; Wei, S.-H.; Stampfl, C. *Phys. Rev. B* **2009**, *79*, 035205−035215.
(40) Sahoo, S.; Husale, S.; Colwill, B.; Lu, T.-M.; Nayak, S.; Ajayan, P. M. *ACS Nano* **2009**, *3*, 3935–3944.

JA106788X